Confining functional nanoparticles into colloidal imine-based COF spheres by a sequential encapsulation-crystallization method

David Rodríguez-San-Miguel,[†][a] Amirali Yazdi,[†][b] Vincent Guillerm,[b] Javier Pérez-Carvajal,[b] Víctor Puntes,[b,c] Daniel Maspoch*[b,c] and Félix Zamora*[a,d,e]

Abstract: Here we report a two-step method that enables imparting new functionalities to covalent-organic frameworks by nanoparticle confinement. The direct reaction between 1,3,5-tris(4-aminophenyl)benzene and 1,3,5-benzenetricarbaldehyde in presence of a variety of metallic/metal oxide nanoparticles results in the nanoparticles being embedded in amorphous and non-porous imine-linked polymer organic spheres, **NP@a-1**. Post-treatment reactions of **NP@a-1** with acetic acid under reflux lead to crystalline and porous imine-based COF hybrid spheres, **NP@c-1**. Interestingly, **Au@c-1** and **Pd@c-1** have been found to be catalytically active.

The confinement of metallic and metal oxide nanoparticles (NPs) in porous materials is a fruitful strategy to develop composites in which the porous matrix acts both as a dispersive and protective media for the NPs while providing effective and selective accessibility to them. Thanks to these properties, this class of composites shows promises for myriad applications, including heterogeneous catalysis,[1] sensing,[2] gas storage,[3] plasmonics,[4] remediation,[5] batteries,[6] biocides,[7] magnetic refrigeration,[8] and controlled guest release.[9] To date, different porous materials have been explored for producing these composites, including activated carbon,[10] silica,[11] microporous zeolites,[12] porous organic polymers[13] and, more recently, metal-organic frameworks (MOFs).[14] Among the new porous materials available today, their covalent counterparts covalent-organic frameworks (COFs) are also emerging as attractive candidates for the elaboration of these composites. As MOFs, COFs are attainable in various pore sizes and shapes, with large surface areas and tailored pore surfaces. Despite their challenging crystallization,[15] COFs show better thermal and chemical (e.g. aqueous, alkali and acidic) stability, which can be a crucial feature for certain applications,[16] such as in heterogeneous catalysis, remediation and biomedicine. Recently, NPs have begun to be incorporated in COFs by infiltration of the NP precursors and subsequent growth of the NPs inside the pores.[17] In MOFs, an alternative approach that has proved very productive for making a wide variety of MOF/NP composites is the encapsulation of pre-synthesized NPs into the MOF crystals.[18] This approach allows controlling the size, shape and composition of the NPs and therefore, their inherent properties.[14a] It also allows improving their dispersion and controlling the number and localization of these NPs inside the MOF crystals.[19] Thus far, however, no one has demonstrated yet the ability to apply this approach in COF particles. This is in part because of the incompatibility of the NP chemistry and that used to synthesize and crystallize COFs.

Here, we report a two-step strategy that enables the encapsulation of several types of NPs into imine-based COF spheres (Scheme 1). The first step is based on the encapsulation of NPs into amorphous imine-based spheres under mild conditions. This process resembles the traditional encapsulation technologies widely used for the entrapment of species into colloidal amorphous purely organic or metal-organic polymer spheres.[20]
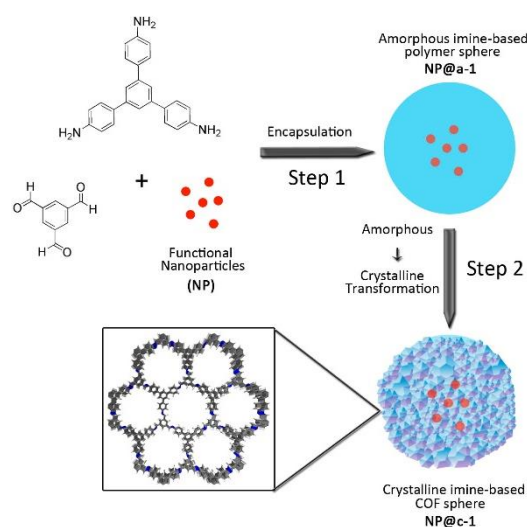
[a]   D.R., Dr. F.Z.
        Departamento de Química Inorgánica and Institute for Advanced
        Research in Chemical Sciences
        Universidad Autónoma de Madrid
        28049 Madrid (Spain).
        E-mail: felix.zamora@uam.es
[b]   A. Y., Dr. V. G., Dr. J. P., Prof. Dr. D. M.
        Catalan Institute of Nanoscience and Nanotechnology (ICN2), CSIC
        and The Barcelona Institute of Science and Technology
        Campus UAB, Bellaterra, 08193 Barcelona, Spain
        E-mail: daniel.maspoch@icn2.cat
[c]   Prof. Dr. D. M.
        ICREA, Pg. Lluís Companys 23, 08010 Barcelona, Spain
[d]   Dr. F.Z.
        Instituto Madrileño de Estudios Avanzados en Nanociencia (IMDEA
        Nanociencia)
        Cantoblanco, 28049 Madrid (Spain).
[e]   Dr. F.Z.
        Condensed Matter Physics Center (IFIMAC)
        Universidad Autónoma de Madrid
        Madrid E-28049 (Spain)

[†] These two authors made equal contribution to this paper.

        Supporting information for this article is given via a link at the end of
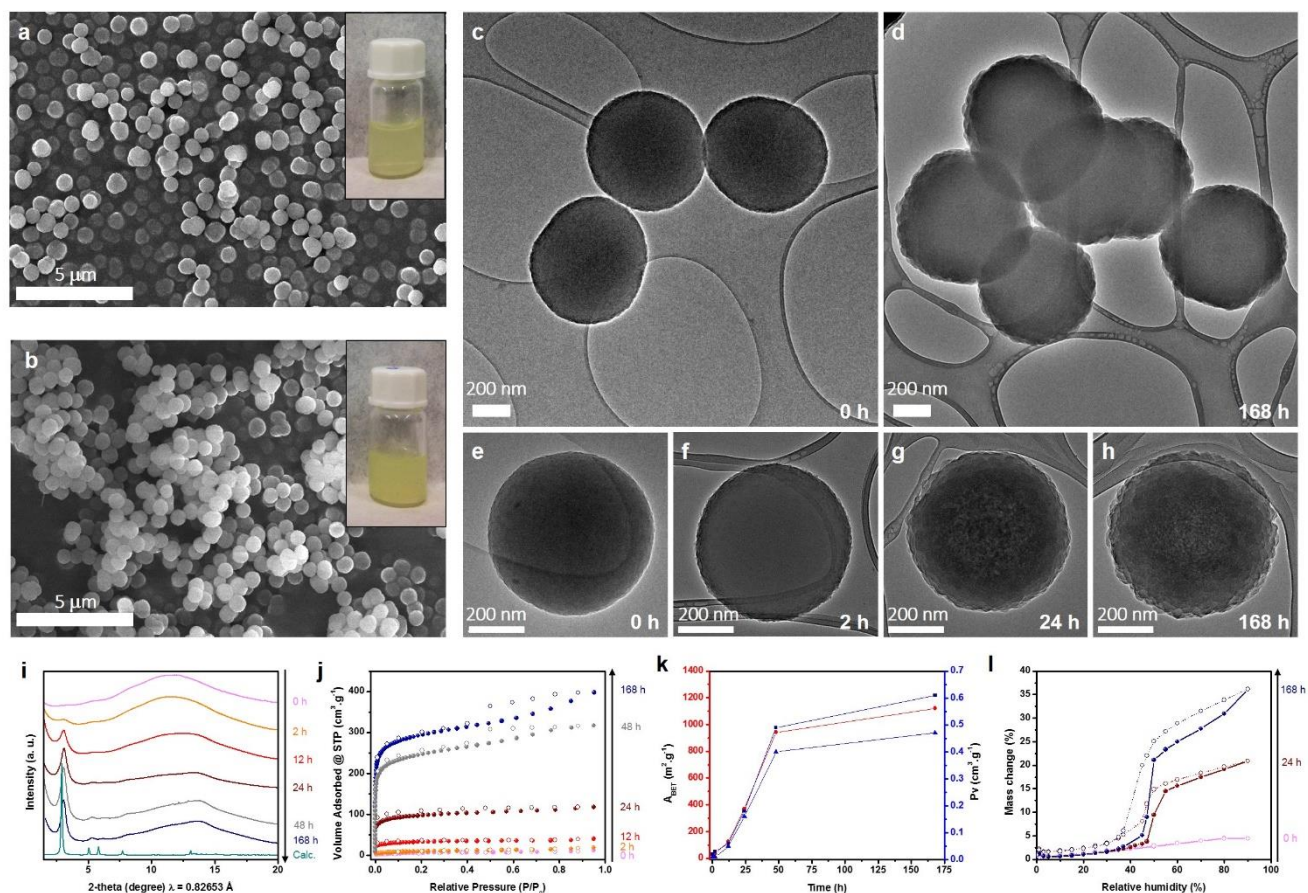   the document.

Figure 1. a,b) Representative FESEM images of **a-1** (a) and **c-1** (b) spheres. Insets show the corresponding photography of an aqueous colloidal solution. c,d) TEM images of **a-1** (c) and **c-1** (d) spheres. e-h) Evolution of the roughness of the COF spheres at t = 0 h (e), 2 h (f), 24 h (g) and 168 h (h). i-l) Evolution of the crystallinity (**i**), porosity (j, k), and water sorption uptake (l) during the amorphous $\Rightarrow$ crystalline transformation. In k, A_{BET} (red), micropore volume (blue) and total pore volume (black). In l, water sorption isotherms of **a-1** (pink), **a-1** treated for 24 h (magenta), and **c-1** (blue).

The second step is based on the possibility to transform solid amorphous imine-like polymers to their crystalline COF analogues by exposing them to acidic conditions at 70 ºC. Initially reported by Dichtel *et al.*,[21] a variation of this method was recently used by Guo *et al.* to coat single ≈ 200-300 nm-in-diameter iron oxide spheres with a layer of an imine-based COF for photothermal therapy.[17] Remarkably, in the present study we show that this second crystallization step preserves the initial colloidal property of the amorphous imine-based spheres and the dispersion, size, shape and properties of the embedded NPs.

The design of our method began with the study of the formation of the amorphous imine-based polymer spheres and their subsequent transformation into their analogue porous COF spheres (see details in ref. [22]). To this end, two trigonal building blocks, 1,3,5-tris(4-aminophenyl)benzene and 1,3,5-benzenetricarbaldehyde, were dissolved in an acetone/acetic acid mixture and stirred for 1 h at room temperature.[22] The resulting yellow suspension was centrifuged (18407 rcf) for 2 min, and the collected solid was finally washed twice with acetone and tetrahydrofuran, and finally dried for 48 h at room

temperature and for 24 h at 150 ºC under vacuum. Field-emission scanning (FESEM) and transmission (TEM) electron microscopy images and X-ray powder diffraction (XRPD) studies revealed that this fast condensation reaction produced the kinetically favorable, amorphous spheres with diameter of *ca.* 600 nm (hereafter called **amorphous-1** or **a-1**; Figure 1a,c and i). The spectroscopic and analytical characterization of **a-1** agrees with those data already reported (Figures S1-S3).[22]

The formation of the more thermodynamically stable long-range ordered structure was then achieved under reversible bond formation conditions. For this, **a-1** spheres were treated with acetic acid containing a controlled amount of water under reflux in a mixture of mesitylene/dioxane for 2, 12, 24, 48 and 168 h. Then, each one of the synthesized solids was collected by centrifugation (2348 rcf), washed with toluene, and dried for 48 h at room temperature and for 24 h at 150 ºC under vacuum. The spectroscopic and analytical characterization of **c-1** does not show any significant change to that observed for its amorphous precursor **a-1** (Figures S1-S4). The evolution of the amorphous $\Rightarrow$ crystalline transformation was then followed by analyzing these solids by TEM, FESEM, XRPD, and gas and

water sorption studies (Figure 1). TEM images showed submicrometric spheres (*ca.* 600 nm diameter) for all samples (Figure 1c-h), thereby confirming that this treatment retains the shape and size of the initial **a-1** spheres. However, a closer look at the texture revealed a gradual increase in the roughness of the material for longer treatment times. XRPD clearly showed a gradual evolution of the crystallinity as a function of time (Figure 1i), with the appearance of peaks that properly match those calculated for the expected eclipsed COF structure (rather than the staggered) (Figure S6).[23] Thus, we assumed that the increase in roughness detected during the transition from **a-1** to the spheres treated for 168 h (hereafter called **crystalline-1** or **c-1**) is due to the formation of crystalline domains based on COF nanolayers that are confined within the spheres (Figure 1a-f).

This phenomenon was further confirmed by the calculation of the apparent Brunauer Emmet Teller (BET) area from N_2 sorption experiments performed at 77 K (Figures S7-12), showing a dramatic, gradual increase (Figure 1j,k) from non-porous ($A_{BET} = 25$ m^2.g^{-1}, $V_t = 0.02$ cm^3.g^{-1}) for **a-1** up to highly porous for **c-1** ($A_{BET} = 1120$ m^2.g^{-1}, $V_t = 0.61$ cm^3.g^{-1}) after 168 h of treatment. The collected isotherms were found to be, according to IUPAC classification, type IV isotherm presenting H_2 type hysteresis loop. This behavior, commonly attributed to the presence of some mesoporosity, is in the present case more likely due to some structural swelling -as sometimes observed in this type of materials[24] or a combination of both.

In light of this porosity, we also investigated the CO_2 sorption (Figure S13) and water vapor sorption (Figure 1l) properties of **a-1** and **c-1**. As many amorphous polymers and despite its non-accessibility to N_2, **a-1** was found to be slightly porous to CO_2, with a total uptake (203 K, 760 Torr) of 3.9 mmol.g^{-1}. As expected, **c-1** material exhibited a much higher total uptake in similar conditions (14.3 mmol.g^{-1}). The heats of adsorption (Qst) derived from the isotherms collected at various temperatures between 258 K and 298 K were found to be comprised between 35 and 20 kJ.mol^{-1} for **a-1** and between 25 and 19 kJ.mol^{-1} for **c-1** (Figures S14,S15). These values are in the expected range of energies for a material without specific group expected to interact with CO_2. The higher Q*st* observed for the amorphous material can be attributed to a smaller pores size (**a-1** is non-porous to N_2).

Water vapor sorption isotherms showed that the amorphous $\Rightarrow$ crystalline transformation induces a gradual transition from hydrophobic to hydrophilic behavior (Figure 1l). Water uptake of **a-1** increased monotonically, achieving a total uptake of only 0.04 g$_{water}$.g$_{COF}^{-1}$. Interestingly, the development of porosity leads to an increase of the uptake up to 0.21 g$_{water}$.g$_{COF}^{-1}$ and 0.37 g$_{water}$.g$_{COF}^{-1}$ after 24 h and 168 h of treatment, respectively. This behavior can be correlated with the gradual structural rearrangement from **a-1** into **c-1** upon treatment. The water isotherm of **c-1** can be ascribed as type V, which is a typical behavior of porous materials with hydrophobic walls.[25]
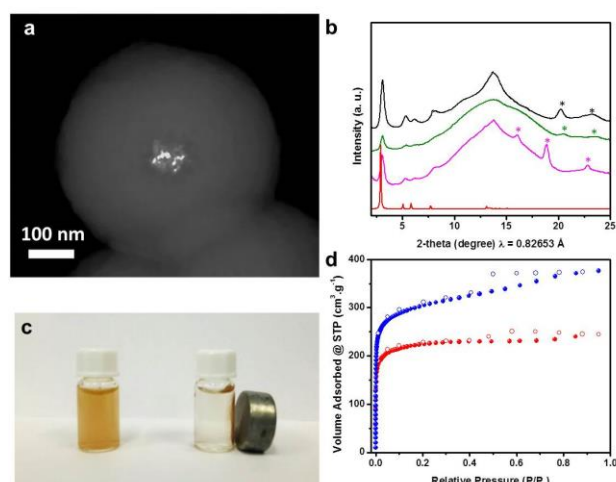

Figure 2. a) HAADF-STEM image of single **Fe₃O₄@c-1** sphere. b) XRPD diagrams of **Fe₃O₄@c-1** (pink), **Au@c-1** (black) and **Pd@c-1** (green) composites in comparison to the simulated for the calculated from the expected eclipsed **c-1** structure (red). Stars highlight the presence of the characteristic peaks of the NPs. c) Visual observation of the magnetic nature of **Fe₃O₄@c-1** spheres. d) N_2 sorption isotherms of **c-1** (blue) and **Fe₃O₄@c-1** spheres (red).

Once we confirmed that the chemical treatment leading to the rearrangement of the amorphous, non-porous **a-1** spheres into crystalline, highly porous **c-1** spheres can take place, we envisioned the use of the two-step process to confine NPs into COFs. In this process, the fast formation of **a-1** spheres should allow the encapsulation of NPs at room temperature. Then, because the NPs are encapsulated and protected, the amorphous $\Rightarrow$ crystalline transformation at high temperatures should occur without compromising the properties of the NPs.

To prove the efficiency of this strategy, we initially started with the encapsulation of Fe_3O_4 NPs (9.8 ± 3.9 nm). These NPs were synthesized using well-established methods, functionalized with polyvinylpyrrolidone (PVP) and dispersed in acetone.[26] These Fe_3O_4 NPs were incorporated into the acetone/acetic acid mixture of the two trigonal building blocks, and the two-step process was reproduced using the above-mentioned conditions. HAADF-STEM micrographs and XRPD studies of the solids collected after the first and second step showed the successful formation of **Fe₃O₄@a-1** and **Fe₃O₄@c-1** submicron spheres containing Fe_3O_4 NPs dispersed mostly in their center (Figure 2a,b and Figure S16). The chemical composition of **Fe₃O₄@c-1** spheres determined by energy-dispersive X-ray (EDX) microanalysis revealed that every sphere contained iron, oxygen, nitrogen and carbon (Figure S18). The content of Fe in the composites was estimated by ICP-OES, from
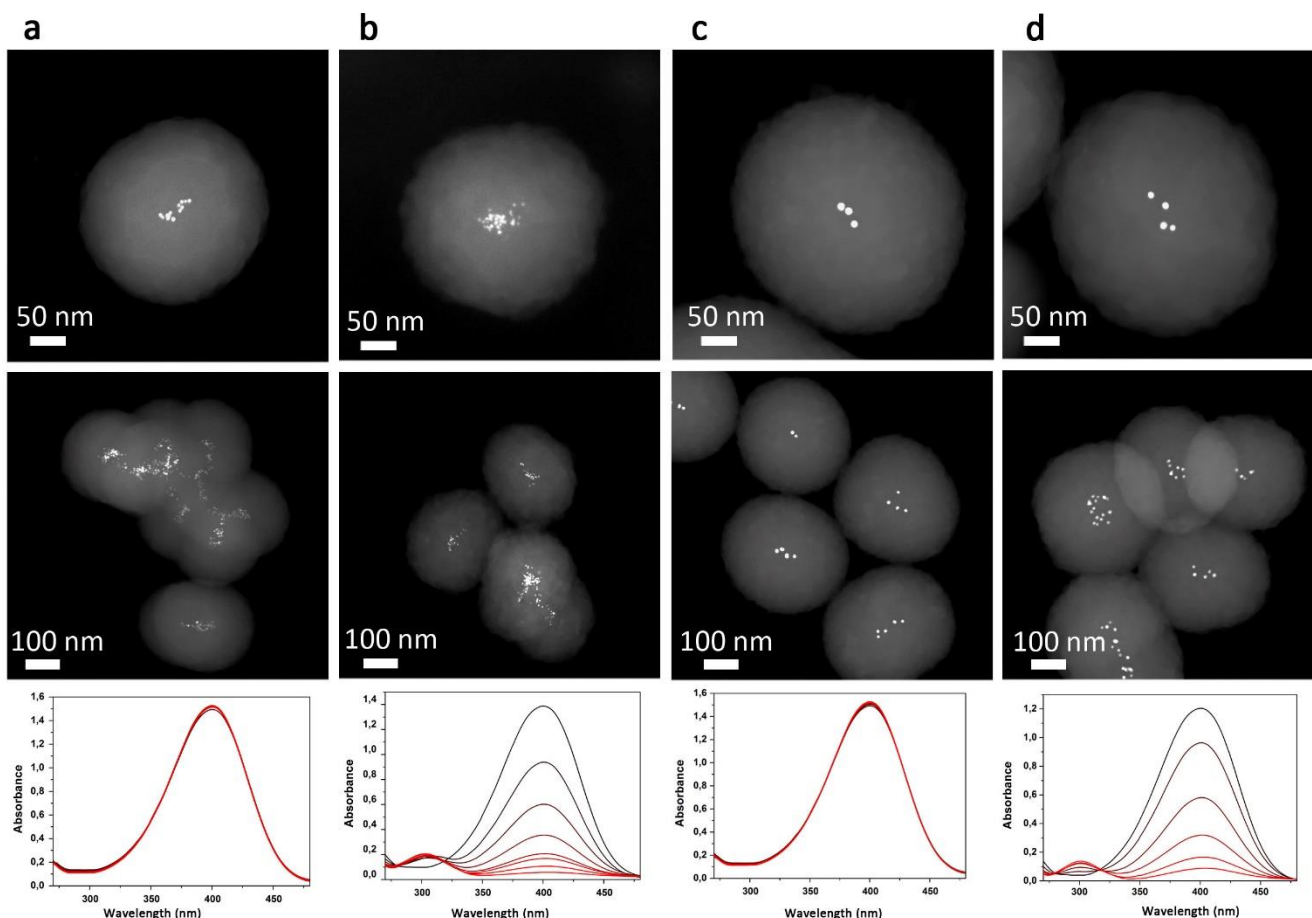
Figure 3. HAADF-STEM images (first row: single sphere; second row: general view) of **Pd@a-1** (a), **Pd@c-1** (b), **Au@a-1** (c), and **Au@c-1** (d) composites. Third row shows the UV-vis evolution of 4-NP reduction using the corresponding composites as catalysts. Each spectrum was collected in intervals of 2 min.

which a Fe_3O_4 NP content of 7.6 % w/w in the composite was determined. In addition, colloidal **Fe$_3$O$_4$@c-1** spheres showed magnetic attraction when they were exposed to a magnet (Figure 2c). So, it can be concluded that NPs encapsulated within the COF spheres are the initial Fe_3O_4 NPs, and therefore, that the two-step process does not modify the properties of the embedded NPs. Also, the permanent porosity of **Fe$_3$O$_4$@c-1** spheres was evaluated by N_2 sorption at 77 K. As expected, the sample was found to be porous, with an apparent BET area lower than the **c-1** spheres (Figure 2d, A_{BET} = 880 $m^2.g^{-1}$, V_t = 0.38 $cm^3.g^{-1}$).

We then extended the use of this process to the encapsulation of other types of NPs. Using the same strategy, **c-1** spheres containing Au (9.0 ± 2.4 nm) and Pd (3.3 ± 1.1 nm) NPs were prepared (Figure 3). As shown by XRPD measurements, both composites exhibited the characteristic peaks of **c-1** as well as the diffraction peaks associated to the NPs (Figure 2b). Moreover, EDX microanalysis confirmed the presence of Au and Pd in the **Au@c-1** and **Pd@c-1** composites, respectively (Figures S20 and S22).

This type of metallic NP/COF composites should be very useful for heterogeneous catalysis. However, for this to be a reality, the porous COF matrix should allow the accessibility of molecules to the embedded NPs. As a proof-of-concept, we studied this accessibility using both **Au@c-1** and **Pd@c-1**

composites for the catalytic reduction of 4-nitrophenol (4-NP) into 4-aminophenol (4-AP) in the presence of $NaBH_4$ as a reducing agent. The catalytic reactions were conducted by mixing two aqueous solutions of $NaBH_4$ and 4-NP with an aqueous dispersion of **Pd@c-1** (Pd: 1.1 % w/w) or **Au@c-1** (Au: 3.5 % w/w), and followed by UV−vis spectroscopy (Figure 3). As control experiments, we also reproduced the same reaction using **c-1** (without NPs) and amorphous **Au@a-1** and **Pd@a-1** hybrids as catalyst. In these latter cases, none of them showed catalytic activity (Figure 3 and Figure S24). For the **Au@c-1** and **Pd@c-1** hybrids, however, their catalytic activity was confirmed by the reduction of the peak at 400 nm, as well as the appearance of a new peak at 305 nm, corresponding to 4-AP (Figure 3). 4-NP was fully reduced into 4-AP after 10 min for **Au@c-1** and 14 min for **Pd@c-1.** These results are comparable to previously reported reductions of 4-NP by NP/MOF (mainly, ZIF-8 and UiO-66) hybrids but slightly less active than a Au@carbon yolk shell nanocomposite,[27] and confirm the accessibility of molecules to the embedded NPs.

In summary, we have demonstrated an efficient and simple two-step procedure to encapsulate several types of NPs into porous and crystalline imine-based COF spheres. This strategy could be extended to a broad range of NPs and mixtures of them, and also to encapsulate molecular species. As a proof-of-concept we have also shown the ability of **Au@c-1** and **Pd@c-1**

hybrids to produce the catalytic reduction of 4-nitrophenol into 4-aminophenol, which confirms the diffusion of reactants and products through the COF spheres to the embedded metallic NPs. This last result suggests potential applications in selective catalysis, remediation and molecular delivery.

Acknowledgements

References

[1]   a) C. Belver, J. Bedia, J. J. Rodriguez, *Appl. Catalysis B* **2015**, *176–177*, 278-287; b) Y. Mei, Y. Lu, F. Polzer, M. Ballauff, M. Drechsler, *Chem. Mater.* **2007**, *19*, 1062-1069; c) S. Ikeda, S. Ishino, T. Harada, N. Okamoto, T. Sakata, H. Mori, S. Kuwabata, T. Torimoto, M. Matsumura, *Angew. Chem. Int. Ed.* **2006**, *118*, 7221-7224.

[2]   M. Segev-Bar, H. Haick, *ACS Nano* **2013**, *7*, 8366-8378.

[3]   C. Zlotea, R. Campesi, F. Cuevas, E. Leroy, P. Dibandjo, C. Volkringer, T. Loiseau, G. Férey, M. Latroche, *J. Am. Chem. Soc.* **2010**, *132*, 2991-2997.

[4]   D. Batra, S. Seifert, L. M. Varela, A. C. Y. Liu, M. A. Firestone, *Adv. Funct. Mater.* **2007**, *17*, 1279-1287.

[5]   a) J. Yang, H. Zhang, M. Yu, I. Emmanuelawati, J. Zou, Z. Yuan, C. Yu, *Adv. Funct. Mater.* **2014**, *24*, 1354-1363; b) F. He, D. Zhao, J. Liu, C. B. Roberts, Ind. Eng. Chem. Res. **2007**, *46*, 29-34; c) S. Saha, A. Pal, S. Kundu, S. Basu, T. Pal, *Langmuir* **2010**, *26*, 2885-2893.

[6]   R. Zou, Q. Liu, G. He, M. F. Yuen, K. Xu, J. Hu, I. P. Parkin, C.-S. Lee, W. Zhang, *Adv. Energy Mater.* **2016**, 1601363-n/a.

[7]   a) P. Lalueza, D. Carmona, M. Monzón, M. Arruebo, J. Santamaría, *Micropor. Mesopor. Mater.* **2012**, *156*, 171-175; b) J. Pérez-Carvajal, P. Lalueza, C. Casado, C. Téllez, J. Coronas, *Appl. Clay Sci.* **2012**, *56*, 30-35.

[8]   A. Zeleňáková, P. Hrubovčák, O. Kapusta, V. Zeleňák, V. Franco, *Appl. Phys. Lett.* **2016**, *109*, 122412.

[9]   a) C.-Y. Lai, B. G. Trewyn, D. M. Jeftinija, K. Jeftinija, S. Xu, S. Jeftinija, V. S. Y. Lin, *J. Am. Chem. Soc.* **2003**, *125*, 4451-4459; b) P. Yang, S. Gai, J. Lin, *Chem. Soc. Rev.* **2012**, *41*, 3679-3698; c) K. H. Min, K. Park, Y.-S. Kim, S. M. Bae, S. Lee, H. G. Jo, R.-W. Park, I.-S. Kim, S. Y. Jeong, K. Kim, I. C. Kwon, *J. Control. Release* **2008**, *127*, 208-218.

[10]   a) C. He, S. Wu, N. Zhao, C. Shi, E. Liu, J. Li, *ACS Nano* **2013**, *7*, 4459-4469; b) M. Kim, K. Sohn, H. B. Na, T. Hyeon, *Nano Lett.* **2002**, *2*, 1383-1387.

[11]   a) F. Caruso, M. Spasova, V. Salgueiriño-Maceira, L. M. Liz-Marzán, *Adv. Mater.* **2001**, *13*, 1090-1094; b) J. Kim, J. E. Lee, J. Lee, J. H. Yu, B. C. Kim, K. An, Y. Hwang, C.-H. Shin, J.-G. Park, J. Kim, T. Hyeon, *J. Am. Chem. Soc.* **2006**, *128*, 688-689.

[12]   a) G. Yang, N. Tsubaki, J. Shamoto, Y. Yoneyama, Y. Zhang, *J. Am. Chem. Soc.* **2010**, *132*, 8129-8136; b) J. Chen, Z. Feng, P. Ying, C. Li, *J. Phys. Chem. B* **2004**, *108*, 12669-12676.

[13]   A. G. Skirtach, C. Dejugnat, D. Braun, A. S. Susha, A. L. Rogach, W. J. Parak, H. Möhwald, G. B. Sukhorukov, *Nano Lett.* **2005**, *5*, 1371-1377.

[14]   a) G. Lu, S. Li, Z. Guo, O. K. Farha, B. G. Hauser, X. Qi, Y. Wang, X. Wang, S. Han, X. Liu, J. S. DuChene, H. Zhang, Q. Zhang, X. Chen, J. Ma, S. C. J. Loo, W. D. Wei, Y. Yang, J. T. Hupp, F. Huo, *Nature Chem.* **2012**, *4*, 310-316; b) P. Falcaro, R. Ricco, A. Yazdi, I. Imaz, S. Furukawa, D. Maspoch, R. Ameloot, J. D. Evans, C. J. Doonan, *Coord. Chem. Rev.* **2016**, *307, Part 2*, 237-254; c) C. M. Doherty, D. Buso, A. J. Hill, S. Furukawa, S. Kitagawa, P. Falcaro, *Acc. Chem. Res.* **2014**, *47*, 396-405; d) M. Mukoyoshi, H. Kobayashi, K. Kusada, M. Hayashi, T. Yamada, M. Maesato, J. M. Taylor, Y. Kubota, K. Kato, M. Takata, T. Yamamoto, S. Matsumura, H. Kitagawa, *Chem. Commun.* **2015**, *51*, 12463-12466.

[15]   D. Beaudoin, T. Maris, J. D. Wuest, *Nature Chem.* **2013**, *5*, 830-834.

[16]   J. L. Segura, M. J. Mancheno, F. Zamora, *Chem. Soc. Rev.* **2016**, *45*, 5635-5671.

[17]   J. Tan, S. Namuangruk, W. F. Kong, N. Kungwan, J. Guo, C. C. Wang, *Angew. Chem. Int. Ed.* **2016**, *55*, 13979-13984.

[18]   G. Lu, S. Z. Li, Z. Guo, O. K. Farha, B. G. Hauser, X. Y. Qi, Y. Wang, X. Wang, S. Y. Han, X. G. Liu, J. S. DuChene, H. Zhang, Q. C. Zhang, X. D. Chen, J. Ma, S. C. J. Loo, W. D. Wei, Y. H. Yang, J. T. Hupp, F. W. Huo, *Nature Chem.* **2012**, *4*, 310-316.

[19]   a) L. Chen, Y. Peng, H. Wang, Z. Gu, C. Duan, *Chem. Commun.* **2014**, *50*, 8651-8654; b) S. Li, F. Huo, *Small* **2014**, *10*, 4371-4378.

[20]   a) I. Imaz, J. Hernando, D. Ruiz-Molina, D. Maspoch, *Angew. Chem. Int. Ed.* **2009**, *48*, 2325-2329; b) Y. Zhang, D. Rochefort, *J. Microencapsul.* **2010**, *27*, 703-713.

[21]   B. J. Smith, N. Hwang, A. D. Chavez, J. L. Novotney, W. R. Dichtel, *Chem. Commun.* **2015**, *51*, 7532-7535.

[22]   D. Rodríguez-San-Miguel, J. J. Corral-Pérez, E. Gil-González, D. Cuellas, J. Arauzo, V. M. Monsalvo, V. Carcelén, F. Zamora, *CrystEngComm., DOI: 10.1039/C6CE02200F.* **2016**.

[23]   A. D. Ruigomez, D. Rodriguez-San-Miguel, K. C. Stylianou, M. Cavallini, D. Gentili, F. Liscio, S. Milita, O. M. Roscioni, M. L. Ruiz-Gonzalez, C. Carbonell, D. Maspoch, R. Mas-Balleste, J. L. Segura, F. Zamora, *Chem.Eur. J.* **2015**, *21*, 10666-10670.

[24]   a) R. Dawson, A. I. Cooper, D. J. Adams, *Prog. Polym. Sci.* **2012**, *37*, 530-563; b) V. Guillerm, L. J. Weselinski, M. Alkordi, M. I. H. Mohideen, Y. Belmabkhout, A. J. Cairns, M. Eddaoudi, *Chem. Commun.* **2014**, *50*, 1937-1940.

[25]   a) M. F. de Lange, K. J. F. M. Verouden, T. J. H. Vlugt, J. Gascon, F. Kapteijn, *Chem. Rev.* **2015**, *115*, 12205-12250; b) S. Paranthaman, F.-X. Coudert, A. H. Fuchs, *Phys. Chem. Chem. Phys.* **2010**, *12*, 8124-8130; c) J. Canivet, J. Bonnefoy, C. Daniel, A. Legrand, B. Coasne, D. Farrusseng, *New J. Chem.* **2014**, *38*, 3102-3111.

[26]   X. Liu, Z. Ma, J. Xing, H. Liu, *J. Magn. Magn. Mater* **2004**, *270*, 1-6.

[27]   a) Z. Li, H. C. Zeng, *Chem. Mater.* **2013**, *25*, 1761-1768; b) W. Zhang, G. Lu, C. Cui, Y. Liu, S. Li, W. Yan, C. Xing, Y. R. Chi, Y. Yang, F. Huo, *Adv. Mater.* **2014**, *26*, 4056-4060; c) R. Lui, S. M. Mahurin, C. Li, R. R. Unocic, J. C. Idrobo, H. Gao, S. J. Pennycook, S. Dai, *Angew. Chem. Int. Ed.* **2011**, 50, 6799-6802.

Entry for the Table of Contents

COMMUNICATION

A simple two-step method allows encapsulating several functional nanoparticles into porous and crystalline imine-based COF spheres. The embedded nanoparticles are accessible to external species, thereby expanding the scope of these COF-nanoparticle hybrids to applications such as catalysis.
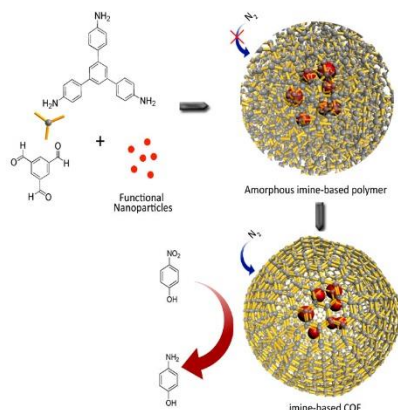
David Rodríguez-San-Miguel, Amirali Yazdi, Vincent Guillerm, Javier Pérez-Carvajal, Víctor Puntes, Daniel Maspoch* and Félix Zamora*

Page No. – Page No.

Confining functional nanoparticles into colloidal imine-based COF spheres by a sequential encapsulation-crystallization method